

Reactivity studies with gold-supported molybdenum nanoparticles

Denis V. Potapenko ^a, Jillian M. Horn ^{a,b}, Robert J. Beuhler ^a,
Zhen Song ^a, Michael G. White ^{a,b,*}

^a Chemistry Department, Brookhaven National Laboratory, Bldg 555, Upton, NY 11973, USA

^b Department of Chemistry, Stony Brook University, Stony Brook, NY 11790, USA

Received 11 August 2004; accepted for publication 21 October 2004

Available online 5 November 2004

Abstract

The reconstructed $(22 \times \sqrt{3})\text{-Au}(111)$ surface was used as a template and inert support for depositing Mo nanoparticles for reactivity studies of desulfurization and the formation of MoS_x nanoparticles. Nanoparticles of Mo were prepared on the Au(111) substrate by two methods: physical vapor deposition (PVD) of Mo and UV-assisted chemical vapor deposition (UV-CVD) through a molybdenum hexacarbonyl precursor. STM studies have shown that the Mo nanoparticles are thermodynamically unstable on the Au(111) surface, and that gold encapsulates Mo at temperatures above 300 K. Reactivity studies using Auger electron spectroscopy (AES) and temperature programmed desorption (TPD) show that bare Mo nanoparticles are very reactive and can cause complete dissociation of hydrogen sulfide, methyl mercaptan, and thiophene. The presence of gold atoms on the Mo nanoparticles modifies their reactivity. In the case of H_2S and CH_3SH , the overall activity for desulfurization is unaffected by gold encapsulation; however, the selectivity to form methane from CH_3SH increased from 20% on bare Mo particles to 60% on gold-covered Mo particles. In contrast, gold-encapsulated Mo nanoparticles are relatively inert towards dissociation of thiophene. We believe that the interaction of R-SH compounds with Au-encapsulated Mo nanoparticles proceeds through intermediacy of surface gold thiolates.

© 2004 Elsevier B.V. All rights reserved.

Keywords: Scanning tunneling microscopy; Thermal desorption spectroscopy; Chemical vapor deposition; Surface structure, morphology, roughness, and topography; Molybdenum; Sulfides; Clusters

1. Introduction

MoS_2 is an important catalyst used in hydrodesulfurization (HDS) processes, where sulfur-containing

* Corresponding author. Tel.: +1 631 344 4345; fax: +1 631 344 5815.

E-mail address: mwhite@bnl.gov (M.G. White).

impurities are removed from petroleum [1]. When present in crude oil, these impurities can cause many undesirable effects, such as releasing environmentally harmful sulfur oxides when the fuel is burned [2]. With new legislation being passed around the globe to reduce the amount of sulfur impurities allowed in fuel [3], HDS catalysts with better efficiency are needed. One approach is to modify the physical (e.g., size) and chemical properties (e.g., alloy, support) of nanostructured forms of the catalytic material in an effort to tailor its catalytic activity and selectivity. It has been shown that nanoparticles may have different chemical properties compared to that of the bulk material [4–6], which results from unique adsorption sites and/or electronic properties of the nanoparticle that are characteristic of its size and chemical environment [6–8].

Recently, Besenbacher and co-workers have shown that the Au(111) surface can be used as a template for MoS₂ nanoparticle growth by physical vapor deposition (PVD) of Mo in the presence of H₂S [9]. The Au(111) surface is used as a substrate due to its chemical inertness and its characteristic $22 \times \sqrt{3}$ herringbone surface reconstruction which provides a template for nanoparticle growth [10]. Strain relief at the Au(111) surface results in a network of dislocation stripes which separate alternating fcc and hcp stacking regions that appear as a zigzag, herringbone structure in STM images [11]. Previous studies have shown that metal clusters (Ni, Fe, Rh, Co, Mo and Pd) preferentially nucleate at the elbows of the herringbone structure when deposited by PVD [12–19]. Mo nanoparticles are stable on gold surfaces since these two metals are mutually insoluble according to the phase diagram [20]. In the case of Mo PVD on Au(111), the resulting array of nanoclusters can be sulfided to produce relatively monodispersed MoS₂ islands [9,21]. In more recent studies, Mo nanoparticles on Au(111) have been prepared using chemical vapor deposition (CVD) of a molybdenum hexacarbonyl (Mo(CO)₆) precursor [17,22]. In contrast to PVD, these clusters were found to be mobile when deposited, forming three-dimensional ramified cluster islands [17] or concentrating at the step edges [22].

In this work, we report on the preparation and reactivity of Mo nanoparticles on Au(111). Qualitative data on the morphology and growth of the Mo and MoS_x nanoparticles is presented through STM images. We find that nanoparticles of bare Mo are thermodynamically unstable on the Au(111) surface and that gold atoms move to the Mo surfaces at temperatures above 300 K. Upon sulfiding, the gold is expelled from the particles and moves back to the terraces. Quantitative measurements of this effect have been completed using Auger electron spectroscopy (AES). The reactivities of bare and gold-covered Mo nanoparticles prepared by PVD on Au(111) were studied using simple HDS test molecules (thiophene, methanethiol, and hydrogen sulfide). Thiophene is a frequently used test molecule for HDS process and is important because it is the simplest of the cyclic hydrocarbons that are resilient toward HDS [23,24]. Reaction products were monitored with temperature programmed desorption (TPD) measurements, and the surface species were characterized using AES. The presence of gold atoms on the Mo nanoparticles modifies their reactivity. In the case of H₂S and CH₃SH, the overall activity for desulfurization is unaffected by gold encapsulation; however, the selectivity to form methane versus deposited carbon increases for CH₃SH decomposition. By contrast, gold-encapsulated Mo nanoparticles exhibit little activity for the dissociation of thiophene.

2. Experimental

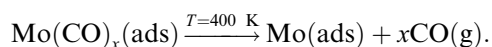
2.1. STM experiments

The STM experiments were carried out in an ultrahigh vacuum system equipped with a scanning tunneling microscope (STM, Omicron), a sputter gun, LEED/Auger and e-beam evaporator (Oxford Applied Research). A preparation chamber was used for sample cleaning and preparation with a directed doser used for chemical vapor deposition. The Au(111) surface was cleaned by cycles of sputtering with Ne⁺ (1 keV) at 520 K, followed by annealing to approximately 900 K until the surface was determined to be clean, with

well-defined terraces and herringbone reconstruction observed in STM images. Molybdenum particles were deposited by physical vapor deposition (PVD) using an e-beam evaporator and a UV-assisted chemical vapor deposition (UV-CVD) procedure previously demonstrated for Mo deposition on Ru(001), Rh(100), Ag(111) and graphite [25–28] surfaces. The UV-CVD procedure involves dosing the Mo(CO)₆ precursor on the gold surface at less than 150 K, followed by exposure to UV light ($\lambda = 300$ nm). The latter was generated by a monochromator-equipped He–Xe arc-lamp (Oriental) and induces partial dissociation of the precursor, i.e.,



The excitation wavelength ($\lambda = 300$ nm) corresponds to a maximum in the adsorption spectrum of Mo(CO)₆ [29], and the UV dose (10 mW/cm² for 2 min) was determined by monitoring the CO desorption kinetics as a function of UV fluence and exposure time [25–28]. Following UV irradiation, the sample was heated to 400 K to remove the remaining CO



The Mo(CO)₆ precursor (Alfa Aesar) was held in an independently pumped glass tube at room temperature, which was pumped out briefly before each dose. For sulfidation, the formed nanoparticles were exposed to 50 L of D₂S (Cambridge Isotope Laboratories) while the sample was kept at 520 K, followed by annealing to 670 K. All STM images were acquired with a tungsten tip at room temperature.

2.2. Reactivity experiments

Reactivity experiments were carried out on a separate ultrahigh vacuum system equipped with a quadrupole mass spectrometer (Extrel), Auger spectrometer (Physical Electronics), a metal evaporation source (Oxford Applied Research), and a sputter gun (LHK). The Au(111) surface was cleaned by sputtering cycles of Ne⁺ (1 keV), followed by annealing to 850 K. The surface was determined to be clean with AES. Molybdenum

was deposited on the Au(111) surface by PVD using an e-beam evaporator similar to that employed in the STM studies. The deposition rates of the evaporator source were calibrated using a quartz microbalance. A directed doser was used to expose the surface to thiophene (Aldrich), methanethiol (Matheson), and hydrogen sulfide (Matheson). The liquid thiophene sample was held in a glass container and degassed by multiple freeze-thaw cycles (with liquid nitrogen) while pumping. The surface coverages of S-containing organic compounds are reported in “single layers”. This is the coverage, above which the onset of multilayer desorption of a given compound from the Au(111) surface occurs. The reactivity was studied by temperature programmed desorption (TPD) and AES. During the TPD measurements, multiple masses were monitored simultaneously with a differentially pumped quadrupole mass spectrometer at a heating rate of 2 K/s. The sample temperature was measured with a K-type thermocouple in direct contact with the gold sample.

3. Results and discussion

3.1. Gold encapsulation of Mo particles on Au(111)

Thermal desorption studies have shown that the chemical properties of freshly prepared Mo/Au(111) surfaces are qualitatively different than that of the same surfaces that have been annealed. Specifically, the surfaces that were prepared by PVD of Mo on a cold (~ 100 K) Au(111) sample caused complete dissociation of all test molecules tried (H₂S, CH₃SH, and C₄H₄S). However, after a first TPD run with any of the above compounds, the surface was significantly passivated, and subsequent TPD experiments on the same surface exhibited different reactivity patterns, as reported in the next section. Here, we report the results of an investigation into the origin of this passivation effect. Experiments have shown that the observed change in surface chemical properties does not depend on the amount of the substance deposited for the first TPD run. Moreover, heating of a freshly prepared Mo/Au(111) surface to temperatures

above 400 K without exposure to any substance led to the same passivation effect. These observations suggest that the passivation of the Mo/Au(111) surface is not caused by carbon or sulfur deposition from the dissociation of adsorbed compounds, but rather is a result of a temperature-induced structural change on the Mo/Au(111) surface.

Fig. 1 shows AES peak height ratios of Mo (190 eV) versus Au (74 eV) for the Au(111) surface, on which approximately 1.5 ML of Mo was deposited by PVD at 100 K. In a set of separate experiments, this sample was incrementally heated to temperatures up to 800 K with a heating rate of 2 K/s. Cooling of the sample began immediately upon reaching each of the target temperatures. It is seen that the surface Mo/Au ratio decreases with heating of the sample to temperatures above 300 K. The structural transformations responsible for the change in surface Mo/Au ratio appear to be kinetically limited processes, since the ratio does not saturate after successive temperature ramps.

STM studies of the Mo/Au(111) surface morphology give a deeper insight into the temperature-induced structural transformations of this surface. Fig. 2 shows STM images of the Au(111) surface with about 0.2 ML of Mo deposited by the PVD method. Molybdenum from the

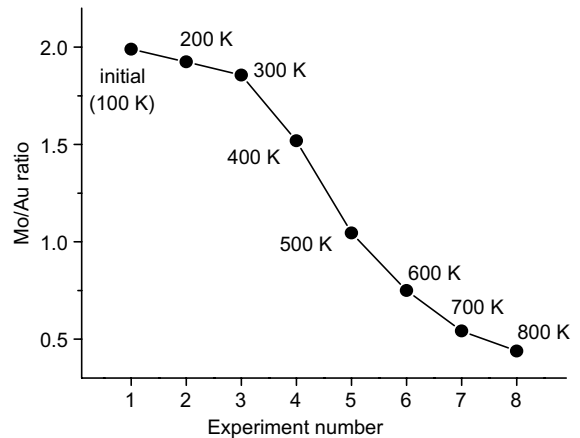


Fig. 1. Mo (190 eV) versus Au (74 eV) AES peak height ratios from Mo deposited by PVD (~1.5 ML) on a Au(111) surface at 100 K (the first point). Points at higher temperatures correspond to consecutive temperature ramps (2 K/s) in which the surface was ramped to a final temperature between 200 and 800 K. AES spectra were taken after each temperature ramp when the sample cooled back to 100 K.

vapor source nucleates preferentially at the elbows of the $22 \times \sqrt{3}$ herringbone surface reconstruction, as can be seen in Fig. 2b. To a lesser extent, Mo nucleates at random sites on the terraces and also at the step edges. This distribution of Mo clusters is qualitatively similar to that obtained previously by Helveg et al. [9]. Cross-sectional analyses of the

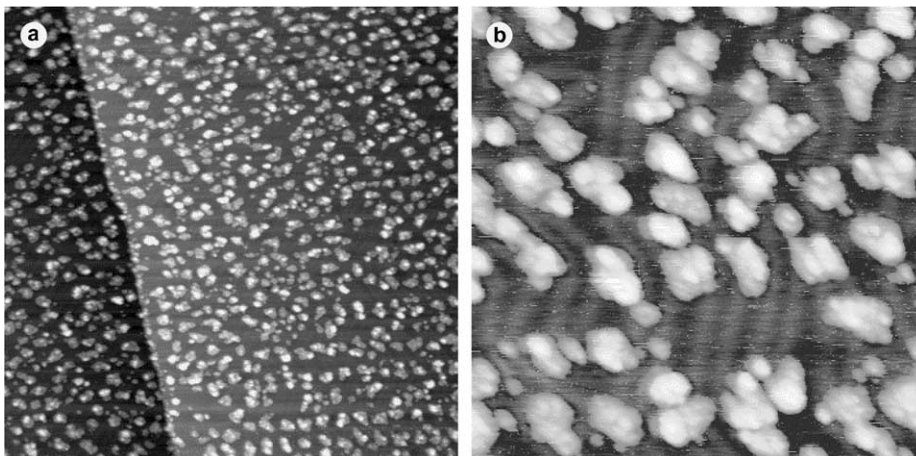


Fig. 2. STM image of the Au(111) surface with about 0.2 ML of Mo deposited by the PVD method. Image sizes: (a) 190×190 nm, (b) 50×50 nm. The underlying $(22 \times \sqrt{3})$ -Au(111) “herringbone” surface reconstruction pattern can be seen in (b).

STM images shows that the average height of the Mo particles is about 4 \AA while the interatomic distance in bulk molybdenum is 2.7 \AA . This suggests that the Mo particles row in a Volmer–Weber fashion on the Au(111) surface, with the formation of 3D clusters at higher Mo coverages [30]. On the basis of the images in Fig. 2, we assume that at Mo coverages of 1 ML (which were used in our reactivity studies) the surface still contains multitudes of partially coalesced Mo nanoparticles with some fraction of the Au(111) surface remaining uncovered.

A UV-assisted chemical vapor deposition (UV-CVD) procedure was also used to deposit Mo, and this approach proved to be more useful for studying Au–Mo interactions on the Au(111) surface. The UV-CVD method of Mo deposition has two important advantages for STM studies over the PVD method used for reactivity studies. First, the UV-CVD procedure allows preferential nucleation of Mo clusters on the step edges of the surface, which is very helpful in tracing the flow of step edges [22]. In contrast, Mo nucleates mostly on terraces when deposited by PVD (see Fig. 2) [9]. Secondly, the UV-CVD procedure can be used to nucleate Mo particles at low temperatures. With PVD, hot Mo atoms from the vapor may cause structural changes in the Au(111) substrate during

the deposition, e.g., site exchange between Au and Mo atoms.

We also note that deposition of Mo on Au(111) by thermal decomposition of $\text{Mo}(\text{CO})_6$ (conventional CVD) leads to particle growth and morphology that are very different from both PVD and UV-CVD. This is seen in a recent STM study by Hrbek and co-workers, where Mo nanoparticles were deposited by exposing the gold surface to $\text{Mo}(\text{CO})_6$ at 500 K [17]. These nanoparticles demonstrate a different growth mechanism, with the Mo clusters forming ramified cluster islands on the terraces and step edges of gold, which were not seen with the UV-CVD method. The complete report on UV-assisted CVD of Mo on Au(111) is given elsewhere [31]. Here we offer only the results directly related to the surface chemistry studies reported in the following sections.

Fig. 3a shows an STM topographic image of the Au(111) surface with 0.03 ML of Mo prepared by UV-CVD, which was then annealed at 525 K for 5 min. As seen in the image, most of the Mo clusters have nucleated at the step edges. Using the rows of the clusters as a reference for the original positions of the step edges on the surface, one can argue that the “bays”, marked with the white arrows in Fig. 3a, were formed after the clusters have nucleated. The formation of similar etch

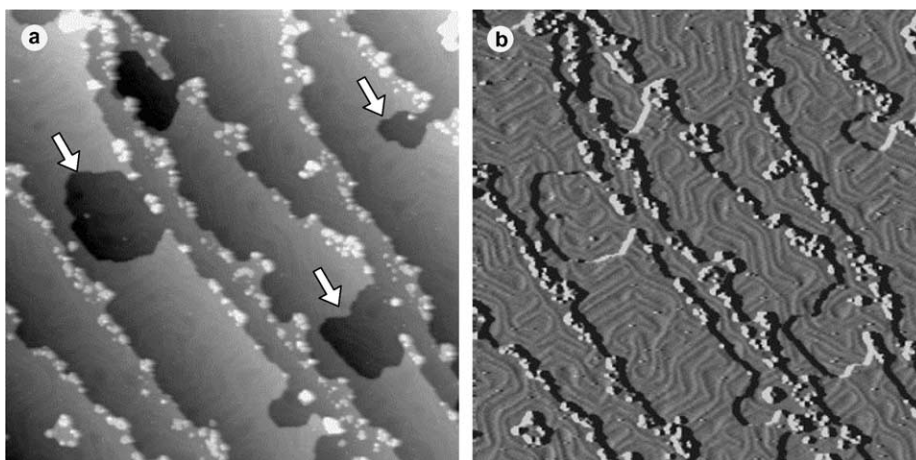


Fig. 3. Topographic (a) and differential (b) representations of the STM image of the Au(111) surface on which ~ 0.03 ML of Mo was deposited through UV-assisted CVD using $\text{Mo}(\text{CO})_6$ as a precursor. The sample was annealed at 520 K before imaging at room temperature. The white arrows point at etching “bays” arising from gold consumption by Mo clusters. Image sizes: 160×160 nm.

holes was observed previously [17,22] and the detailed mechanism for formation of these bays is discussed elsewhere [31]. The presence of the bays indicates consumption of gold atoms somewhere on the surface. Since all the surface areas imaged by STM looked qualitatively similar to that shown in Fig. 3a and no regions of apparent Au segregation could be found, we arrive at the conclusion that the Mo clusters were consuming gold during annealing.

The differential representation in Fig. 3b of the same STM data shows that after annealing, the terraces form an irregular herringbone reconstruction pattern. The origin of the Au(111) surface reconstruction lies in a subtle mismatch between the bulk crystal lattice and the topmost layer [11]. If top layers of the Au terraces (nanoparticle-free areas) contained even a small fraction of alloyed Mo we would not expect to see surface patterns similar to the herringbone reconstruction. The fact that the Au(111) surface reconstruction pattern is irregular, but not lifted completely, suggests that very little Mo migrates to the gold terraces, and prefers to remain in compact clusters after annealing. The same conclusion can be drawn from the Au–Mo phase diagram [20] which shows that the solubility of Mo in Au is extremely low (<1.25 at.% even at 1337 K).

From the same Au–Mo phase diagram [20], these two metals do not form any stable bimetallic compound and the solubility of gold in molybdenum is extremely low (<0.025 at.%). Therefore, it is unlikely that the gold atoms penetrate the Mo clusters but rather segregate on their surface or encapsulate them. This picture is qualitatively consistent with the lower surface free energy of Au (1.62 J/m^2) relative to Mo (2.88 J/m^2) which energetically favors Au capping a Mo surface [32,33]. Additional support is provided by density functional theory (DFT) calculations by Liu et al., showing that a single layer of Mo atoms on a Au(111) surface is less stable than a sandwich structure in which the Mo layer is covered by a surface layer of Au atoms [34]. More sophisticated calculations of the surface segregation energies by Ruban et al., also suggest the tendency of gold to bury molybdenum [35]. These authors also predicted site exchange or intermixing between Mo

nanoparticles with the Au substrate. Our STM results indicate that the Mo–Au interaction results in encapsulation of Mo nanoparticles by Au atoms, migrating from the step edges.

Encapsulation of the deposited metal by the substrate material is usually (but not always) observed when the two metals are immiscible and the surface free energy of the substrate is lower than that of the deposited metal [36]. Encapsulation behavior was reported for Co on Cu(100) [37], on Cu(111) [38], on Ag(100) [39], and on Au(111) [14], Cu on Pb(111) [40], Rh on Au(111) [41], and on Ag(100) [42]. It is interesting to mention that in case of Co/Au(111) system, Co nanoparticles become encapsulated by sinking into the substrate, and the expelled Au proceeds toward the step edges to extend the terraces [14], i.e., the step flow dynamics is just the opposite to what we observe in our studies. On the other hand, encapsulation of Rh nanoparticles deposited on Ag(100) also consumes the substrate material from the step edges and etching “fjords”, analogous to our “bays”, were observed in the STM images [42].

Migration of Au onto the Mo particles is also consistent with the observed kinetic limitations for the encapsulation process at high Mo coverages (>0.5 ML), illustrated by Fig. 1. Since the Au atoms required for encapsulation are supplied from the step edges and not from the terraces or from underneath the Mo clusters, a large surface coverage of clusters would create a hindrance to the step flow. It is possible that at high Mo coverages other mechanisms of gold supply may need to be activated to reach complete encapsulation.

The aforementioned DFT study of Liu et al. [32] also predicts that in the presence of a sulfur adsorbate on a Mo/Au(111) surface, Mo would be pulled back to the surface to form sulfides, MoS_x . This phenomenon was seen in our studies. Fig. 4 shows an STM image of a Au(111) surface with Mo nanoparticles sulfided with D_2S . The surface was prepared by deposition of 0.02 ML of Mo using UV-CVD method then annealed at approximately 520 K for 5 min. With appropriate $\text{Mo}(\text{CO})_6$ deposition and UV exposure conditions, STM images confirmed that the as-prepared Mo/Au(111) surface had a much lower number of

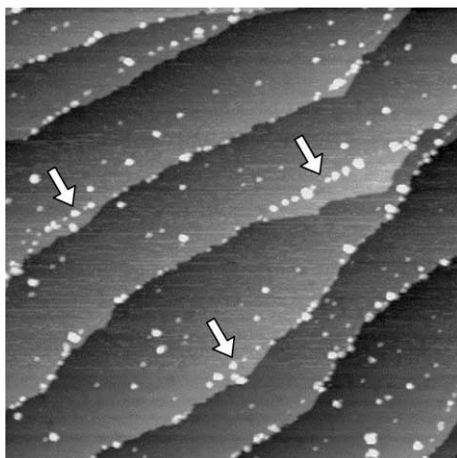


Fig. 4. STM image of the Au(111) surface with about 0.02 ML of Mo deposited in a way similar to that of Fig. 3. The surface then reacted with D₂S at 520 K and annealed at 670 K. The white arrows point at chains of Mo clusters that mark the step positions before the reaction with D₂S. Image size: 240 × 240 nm.

bays in the terraces compared to that in Fig. 3. As before, most of the Mo clusters were situated preferentially on the step edges of the Au(111) surface. The clusters were then sulfided by exposure to D₂S.

The white arrows in Fig. 4 point at chains of Mo clusters that apparently nucleated at the step edges during deposition. Upon D₂S exposure, however, the terraces on the gold surface were extended beyond the lines of the clusters in areas marked with the arrows. We propose that the extended portions of the terraces were formed by the diffusion of gold, expelled from the surface of Mo clusters in the reaction with D₂S.

AES measurements are consistent with the above hypothesis. Sulfur, deposited on a Mo/Au(111) surface binds preferentially to Mo [9,34]. The deposited sulfur atoms should then screen Mo atoms to a greater extent than Au atoms. If no restructuring of the Mo–Au surface is involved in the process of Mo sulfidation, the Mo/Au Auger signal ratio would decrease with increasing S coverage. Experimental data plotted in Fig. 5 exhibits just the opposite trend. The data in Fig. 5 were obtained through a series of consecutive TPD experiments with a Mo/Au(111)

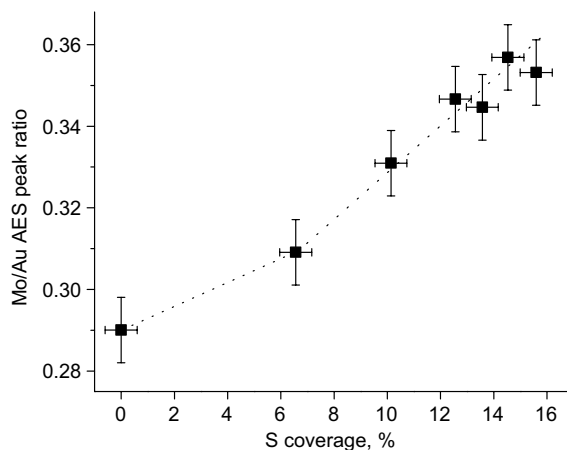


Fig. 5. Measured Mo (190 eV) to Au (74 eV) peak height ratios obtained by AES and plotted versus sulfur content of a Mo/Au(111) surface. The surface was prepared by the deposition of about 0.8 ML of Mo by PVD and annealing to 700 K. Sulfur was deposited in a series of TPD experiments with H₂S (see text for details).

surface (0.8 ML) which was annealed to 700 K and then cooled to 90 K and exposed to H₂S at saturation coverage for each TPD run. Auger spectra were recorded from the initial surface and after each of the TPD experiments. The ratio of Mo (190 eV) versus Au (74 eV) Auger peak heights was then plotted against sulfur coverage. The plot clearly shows that the Mo/Au Auger signal ratio increases as more sulfur is deposited on the surface. This behavior can be explained by having Au atoms expelled from the surface of the Mo nanoparticles by deposited sulfur. Since the expelled Au atoms migrate to the Mo-free areas of the surface, the overall gold AES signal intensity decreases, consistent with the trend seen in Fig. 5.

Although the experiments above provide strong evidence for gold encapsulation of the Mo nanoparticles, the physical structure of the Au-covered Mo surface is not discernable from the STM images. Of particular interest is whether Au simply wets the Mo surface to form islands, i.e., gold caps, or forms a Au/Mo surface alloy with a well-defined morphology and composition. Gold is known to form surface alloys with other early transition metals, e.g., Au/W [43–45] and Au/Ni

[46,47], even though the two metals are immiscible in the bulk (similar to Au/Mo) [48]. Characteristic of such surface alloys are well-ordered $c(2 \times 2)$ surface structures that appear at up to 0.5 ML in which Au atoms are substituted for the substrate atoms in the surface layer. Similar $c(2 \times 2)$ surface structures have been observed for Cu, Ag [49] and Pd [50] overlayers on Mo(100) surfaces and very recent theoretical studies [45] indicate that Cu, Ag and Au will form stable substitutional surface alloys on a Mo(001) surface. In the case of Mo nanoparticles, surface alloying may be favored since nanoparticles are expected to be rich in surface vacancies and defects, e.g., kink and edge sites [51]. The latter are often associated with metal sites of low co-ordination number and high reactivity, and Au substitution at these sites could lead to the observed chemical passivation.

We can use the Mo AES signal attenuation during annealing of a Mo/Au surface to estimate the gold layer thickness on Mo nanoparticles. The largest decrease in the normalized Mo signal, observed after annealing to 800 K, corresponded to attenuation value of 0.65. Taking the inelastic mean free path for an electron in gold as 0.6 nm [52], the observed attenuation corresponds to a 0.26 nm thick gold film or ~ 1.1 ML of gold. This estimation strongly favors Au capping of Mo nanoparticles as opposed to the formation of a Mo–Au surface alloy. Although the above analysis is very approximate, we will refer to this Au migration as encapsulation in the remainder of the paper.

3.2. Reactivity of Mo nanoparticles on Au(111) surface

In this section we report the results of a combined TPD/AES study of chemistry of sulfur-containing compounds on Mo/Au(111) surfaces. Quantitative analysis of the data was performed using TPD peak areas as a measure of the amount of desorbing products. Changes in AES peak intensities, before and after a TPD experiment, were used as a measure of the amounts of deposited elements. Separate studies were carried out on bare and Au-encapsulated Mo nanoparticles, denoted Mo/Au and (Mo)Au respectively.

Molecular hydrogen ($m/e = 2$) was the major desorption product observed in TPD experiments on Mo/Au(111) surfaces exposed to H_2S , CH_3SH , and $\text{C}_4\text{H}_4\text{S}$, as shown in Fig. 6. In these experiments, the surfaces were prepared by PVD of ~ 1 ML of Mo onto a Au(111) surface held at about 85 K, which ensures that the deposited Mo particles were not encapsulated by gold. The test molecules were then deposited at the same sample temperature by means of a directed doser at coverages slightly above a single layer. In the case of CH_3SH , methane desorption was also seen at 290 K, as shown in Fig. 6. The identity of the desorbing product as methane was confirmed by simultaneous monitoring of mass spectrometer

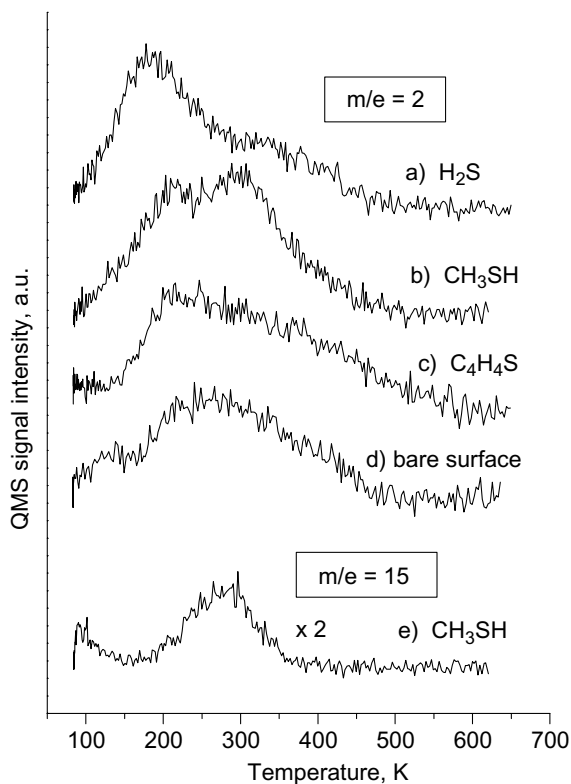


Fig. 6. Thermal desorption spectra from Mo/Au(111) surfaces that were prepared by PVD of 1 ML of Mo on the cold (< 100 K) Au(111) surface followed by dosing with various compounds: (a) H_2S , (b) and (e) CH_3SH , and (c) thiophene. Spectrum (d) was taken after Mo deposition without dosing. Ionic signals for H_2^+ at $m/e = 2$ (a–d) and CH_3^+ at $m/e = 15$ (e) are shown.

signals at $m/e = 15$ and 16 . The ratio of the two signals matched that for the electron fragmentation of CH_4 [53]. No other hydrocarbons were detected in the desorption spectra (except for residual amounts of the unreacted deposited compounds).

Hydrogen desorbs in a very broad temperature range of 100–500 K from all Mo/Au(111) surfaces covered with sulfur compounds. In the case of H_2S , the hydrogen desorption peak has a maximum at 180 K (Fig. 6a) and a broad shoulder at ~ 350 K. Exposing Mo/Au(111) surfaces to $\text{C}_4\text{H}_4\text{S}$ produces H_2 desorption peaks with a much less pronounced maximum at ~ 220 K (Fig. 6c). Finally, hydrogen desorption spectra from Mo/Au(111) surfaces exposed to CH_3SH exhibit a double peak with maxima near 220 and 300 K (Fig. 6b). The fact that the second H_2 desorption peak coincides in temperature with the CH_4 desorption peak suggests a common mechanism for the formation of these two products.

A quantitative analysis of hydrogen desorption was not possible due to the fact that Mo/Au(111) surfaces prepared by PVD were nearly saturated with hydrogen even before deposition of any compound. This can be seen in Fig. 6d, which shows H_2 desorption from a freshly prepared Mo/Au(111) surface. Apparently, hydrogen was co-deposited with Mo during PVD. Molybdenum has a very low vapor pressure and requires high temperatures for deposition (above the melting point of 2883 K). At such high temperatures the evaporative source itself produces hydrogen, raising the partial pressure of hydrogen in the chamber to approximately 2×10^{-8} Torr, in spite of water cooling and preliminary outgassing of the source.

Hydrogen saturation was investigated through experiments in which Mo was deposited in a background pressure of D_2 (up to 3×10^{-7} Torr). Although the D/H ratio on the prepared surfaces could exceed one, the total area of $m/e = 2, 3,$ and 4 TPD peaks from these surfaces was close to that of the $m/e = 2$ TPD peak from a Mo/Au(111) surface that was prepared with no D_2 exposure. This suggests that freshly prepared Mo/Au(111) surfaces were initially saturated with hydrogen. On the other hand, this surface hydrogen did not passivate the Mo/Au(111) surfaces

with regard to any of the S-containing compounds. Indeed, after single TPD runs the sulfur and carbon coverages of the surfaces were close to the corresponding saturation values (see Fig. 8). We also conducted a number of experiments with D_2S deposited on Mo/Au(111) surfaces. A careful analysis of the D/H ratio in the thermal desorption products showed that only about 25% of the desorbing molecular hydrogen (deuterium) originates from the deposited multilayer of H_2S (D_2S). The remainder of the desorbing hydrogen was co-deposited together with molybdenum. Based on AES measurements, the sulfur coverage after such an experiment was 20%, while the maximum coverage obtained after repeated exposures to H_2S was 24%. Together these observations suggest that there are many more adsorption sites for hydrogen than for sulfur on the Mo/Au(111) surface. Another conclusion derived from the isotope experiments is that the hydrogen deposited with Mo and the hydrogen deposited from H_2S (D_2S) are chemically indistinguishable on the surface. Since the D/H ratio remained virtually constant during the entire desorption process, surface hydrogen from both sources must desorb through an identical recombinative process.

The reactivity of Au-encapsulated Mo nanoparticles was also studied. In these experiments, the substrate surfaces were prepared by deposition of about 1 ML of Mo atoms from the PVD source followed by heating of the sample to 600 K. In the case of H_2S , (Mo)/Au(111) surfaces produced molecular hydrogen upon heating (as well as intact H_2S molecules) and the corresponding desorption peak had a temperature profile resembling that of bare Mo particles (Fig. 6a). However, the intensity of the hydrogen peak from the (Mo)/Au(111) surface was at least five times lower. The latter is due to the removal of adsorbed hydrogen that was co-deposited with Mo by annealing the sample prior to H_2S exposure. Since the background levels of hydrogen in the vacuum chamber were elevated during desorption, these $m/e = 2$ TPD signals were not suitable for quantitative analysis (e.g., see Fig. 7).

Thermal desorption products from CH_3SH -covered (Mo)/Au(111) surfaces were also similar to those from the Mo/Au(111) surface, including

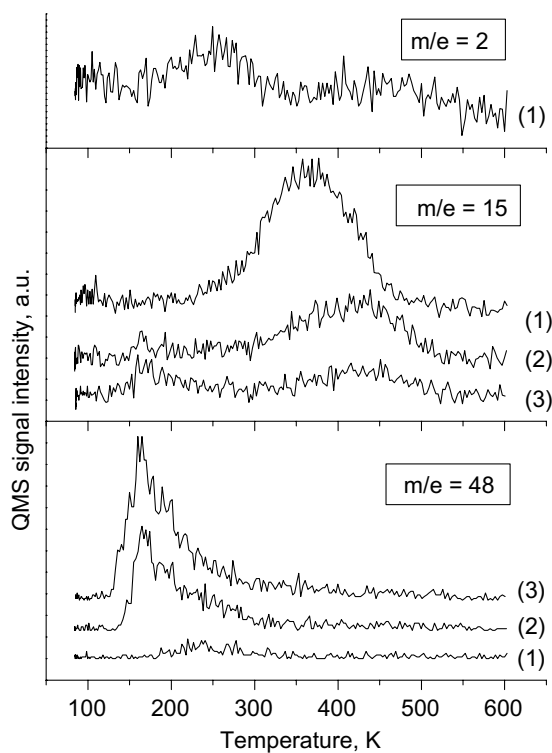


Fig. 7. Three consecutive thermal desorption spectra from a Mo/Au(111) surface that was exposed to a saturated layer of CH₃SH before each experiment. The initial surface was prepared by PVD of 1ML of Mo on a cold (100K) Au(111) surface followed by annealing to 600K. The order of the TPD run is shown in the parenthesis. Ionic signals for H₂⁺, CH₃⁺ and CH₃SH⁺ ($m/e = 2, 15$ and 48) are shown.

methane and molecular hydrogen. Fig. 7 shows three consecutive TPD spectra from the (Mo)/Au(111) surface, for each of which a single layer of CH₃SH was deposited. Only the first spectrum is shown for $m/e = 2$, since in the other two runs the hydrogen peak was not discernable. As can be seen from the figure, subsequent TPD runs resulted in less methane ($m/e = 15$) and a proportional increase in intact CH₃SH desorption ($m/e = 48$), demonstrating saturation of the surface with sulfur (and carbon). It should be noted that mass fragments with $m/e = 15$ (CH₃⁺) also originate from cracking of the parent molecule, CH₃SH, in the ionizer of the mass spectrometer. This can be seen in Fig. 7 as a small peak in the $m/e = 15$ TPD at 160K that replicates the

$m/e = 48$ TPD signal. The broad peak between 300 and 550 K, however, is not accompanied by intact CH₃SH desorption and can be attributed to cracking of the methane desorption product instead. In the case of thiophene-covered (Mo)/Au(111) surfaces, only desorption of intact thiophene molecules could be distinguished, and we do not show the corresponding TPD spectrum.

Analyses of the AES spectra provide a quantitative measure of the extent of the surface reactions. Fig. 8a–c summarize the results in a series of sulfur uptake curves for H₂S, CH₃SH and C₄H₄S. Each of the points in the figures was obtained after a TPD experiment, with height ratios between S (150eV) and Mo (190eV) plotted as a function of the amount of deposited compound. Open circles represent experiments with a bare Mo/Au(111) surface. Only one experiment on bare Mo/Au(111) could be performed since at elevated temperatures Au atoms have migrated to Mo surfaces that have not reacted with sulfur. The filled symbols depict sulfur coverages after successive TPD experiments on (Mo)/Au(111) surfaces that were prepared by annealing to 600K.

As seen in Fig. 8a and b, the reactivities of Mo/Au(111) and (Mo)/Au(111) surfaces toward H₂S and CH₃SH are similar. Apparently, the presence of gold does not significantly hinder the reaction between the sulfur from these compounds and molybdenum. The uptake curves suggest saturation of the surfaces with sulfur, yet no specific saturation sulfur concentration was reached in our experiments. Even with prolonged exposures of the heated surfaces to S-containing compounds the concentrations of sulfur on the surfaces kept increasing, apparently due to the slow process of sulfur diffusion into the bulk of the Mo nanoparticles.

Unlike the other two compounds, thiophene (C₄H₄S) reacts quite differently toward Mo/Au(111) compared with (Mo)/Au(111) surfaces (see Fig. 8c). While thiophene is completely dissociated on bare Mo nanoparticles, only a small fraction of deposited thiophene reacts with gold-encapsulated particles. Additional experiments showed that the reactivity of the (Mo)/Au(111) surface with thiophene depends on the degree of encapsulation of the Mo particles. In four

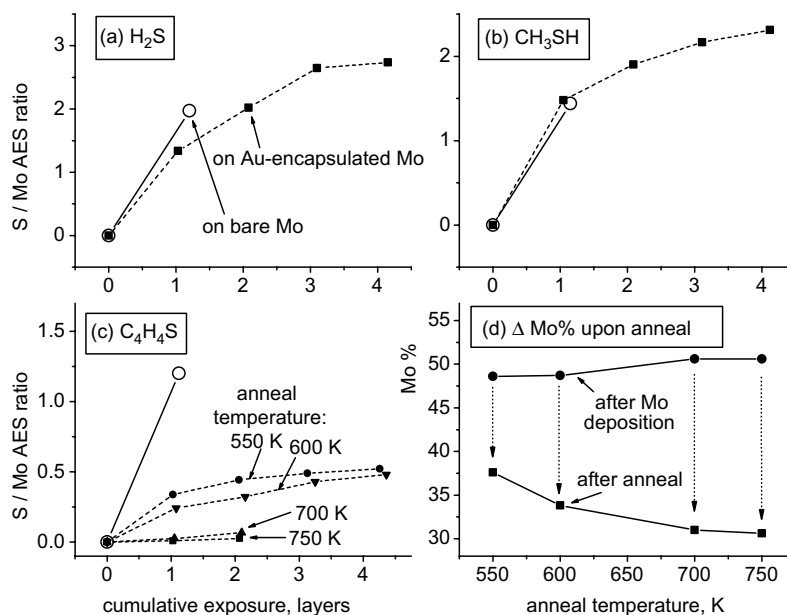


Fig. 8. (a)–(c) Sulfur uptake curves for different compounds on Mo/Au(111) surfaces. Each data point was obtained by deposition of a given compound on a surface followed by thermal desorption. The ratio of the S (152 eV) to Mo (190 eV) AES peak intensities represent the sulfur content of the surfaces. Open circles in each figure correspond to sulfur uptake of bare Mo nanoparticles on Au(111) and closed symbols represent sulfur uptake of Au-encapsulated Mo nanoparticles. Plot (c) shows the uptake curves for a number of (Mo)/Au(111) surfaces prepared by annealing to different temperatures. The change of Mo content of the surfaces during annealing (derived from AES spectra) is shown in plot (d).

experiments, Mo/Au(111) surfaces were prepared in identical ways, and annealed to different temperatures: 550, 600, 700, and 750 K. AES spectra were taken before and after each anneal and the apparent Mo content of the surfaces is plotted in Fig. 8d. The change in Mo AES signal increases as the annealing temperature is increased. Consistent with our earlier observations (see Fig. 1), higher annealing temperatures produce a higher average density of gold caps on the Mo nanoparticles. Reactivity experiments with these four surfaces (Fig. 8c) showed that the uptake of sulfur from the deposited thiophene is greater for the surfaces annealed to lower temperatures. In other words, higher gold coverages make the surfaces more resilient to the reaction with thiophene. In our estimations, less than 1% of thiophene from the deposited layer reacted with the (Mo)/Au(111) surface which was annealed to 750 K. On the other hand, the anneal temperature had no effect on sulfur deposition from H₂S or CH₃SH on gold-encapsulated (Mo)/Au(111) surfaces.

To better understand the reaction mechanisms of sulfur-containing compounds with different Mo/Au(111) surfaces, the amounts of carbon and sulfur deposition were analyzed following surface reactions. The values of the fractional change in the amount of carbon and sulfur on the surface ($\Delta C/\Delta S$) are shown in Table 1. These were calculated as the ratio of increments of the carbon (275 eV) and sulfur (150 eV) AES peak heights di-

Table 1
Elemental ratios of deposited carbon vs. sulfur, $\Delta C/\Delta S$, for the reactions of sulfur-containing compounds with bare and gold-encapsulated Mo nanoparticles on Au(111)

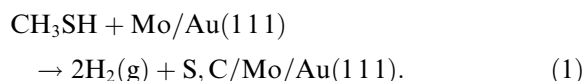
Surface	$\Delta C/\Delta S$ ratio		
	H ₂ S	CH ₃ SH	C ₄ H ₄ S
Mo/Au(111) (bare)	0.0 ± 0.1	0.8 ± 0.2	4.6 ± 0.4
(Mo)/Au(111) (encapsulated)	0.1 ± 0.2	0.4 ± 0.2	4.1 ± 0.4

The ΔC and ΔS values were derived from AES spectra before and after the reactions and are proportional to the number densities of deposited surface carbon and sulfur (normalized to the AES spectrum of CS₂).

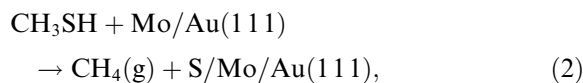
vided by the same ratio that was obtained in a calibration experiment with CS₂ deposited on Au(111) surface (divided by two to account for the S:C ratio in CS₂). Calculated in this way, the $\Delta C/\Delta S$ values reflect the actual atomic ratios of the elements deposited in the TPD experiments. The numbers presented in Table 1 were obtained by averaging over a number of $\Delta C/\Delta S$ values from different experiments (from 3 to 23 for different compounds) and the reported uncertainties are mean square deviations of the averaged samples.

Since H₂S does not contain carbon, the $\Delta C/\Delta S$ for decomposition of this molecule is expected to be equal to zero. This is what we see in Table 1. The first H₂S column of the table shows that undesirable carbon contamination of the sample (due to reaction with the background CO, for instance) is very small in our TPD experiments.

The C:S ratio in CH₃SH is one, therefore, if CH₃SH were to dissociate completely and produce only hydrogen, then the $\Delta C/\Delta S$ ratio would be equal to one according to the reaction,



On the other hand, if CH₃SH were to react with the surface with the deposition of S and desorption of CH₄, i.e.,



then the expected $\Delta C/\Delta S$ ratio would be equal to zero. The $\Delta C/\Delta S$ values for the reaction of CH₃SH with Mo/Au(111) and (Mo)/Au(111) surfaces lie between zero and one, implying that both processes (1) and (2) occur upon heating the sample. A comparison of the TPD peak areas for molecular hydrogen and methane correlate well with the numbers in Table 1. In the case of bare Mo nanoparticles, $\Delta C/\Delta S = 0.8$, which implies the hydrogen producing pathway (1) is preferred, while the partial dissociation pathway (2) is more prominent in the case of gold-encapsulated molybdenum ($\Delta C/\Delta S = 0.4$).

Although the overall activity of the Mo nanoparticles towards C₄H₄S depends strongly on the degree of Au encapsulation (Fig. 8c), the $\Delta C/\Delta S$

ratios for thermal reaction with both Mo/Au(111) and (Mo)/Au(111) surfaces are somewhat above four. This number is consistent with the 4:1 carbon to sulfur stoichiometry and assuming thiophene undergoes complete dissociation on Mo/Au(111) surfaces. The results of our TPD experiments with thiophene are consistent with complete dissociation, since we have never observed any desorption product other than H₂ and intact C₄H₄S. The fact that the $\Delta C/\Delta S$ values are above four (and in one case it is even beyond the uncertainty range) may be explained by imperfect calibration. For example, if some of the molecules in the CS₂ multilayer used in calibrations are oriented normally to the surface, sulfur atoms would screen the AES signal from carbon atoms. This would lower the observed $\Delta C/\Delta S$ ratio for the CS₂ calibration runs and result in overestimated $\Delta C/\Delta S$ ratios for the other compounds.

Comparison of our results with published reactivity studies of Mo and Au surfaces brings a perspective that allows a mechanistic interpretation of the experimental data. Overall, the reactivity patterns of S-containing compounds on bare Mo nanoparticles on the Au(111) surface are very similar to that of close-packed Mo surfaces. Similar to our results for bare Mo particles, molecular hydrogen was the only desorption product from thiophene-exposed Mo(110) [24] and Mo(100) surfaces [54,55]. It is interesting to mention that reactions of thiophene analogues with higher hydrogen content do produce gaseous hydrocarbons on the Mo(110) surface: butadiene in the case of 2,5-dihydrothiophene [56] and butane and butene in the case of tetrahydrothiophene [57]. In our experiments, however, no gaseous hydrocarbons were formed with thiophene, even though the Mo/Au(111) surfaces were pre-saturated with hydrogen.

Methanethiol (CH₃SH) deposited on the Mo(110) surface behaves very similarly to what is observed in our experiments with the Mo/Au(111) surface. Specifically, about 40% of the methanethiol deposited on Mo(110) forms methane according to reaction (2), while the rest non-selectively decomposes to form hydrogen, as in reaction (1) [58]. Inspection of Table 1 shows that on the Mo/Au(111) surface only about 20% of the

CH_3SH decomposes to yield methane with the rest undergoing complete decomposition. This result is reasonable since we expect the Mo nanoparticles to be more active towards complete decomposition (reaction (1)) than the low-index Mo(110) surface due to the higher density of reactive edge sites or other co-ordinatively unsaturated sites. Again, we should note that the low methane production yields were observed *in spite* of the abundance of pre-adsorbed hydrogen on the Mo/Au(111) surface.

On the other hand, methane production from deposited methanethiol increases to 60% on Au encapsulated Mo particles compared to 20% on bare Mo/Au(111) particles and 40% on Mo(110). In this respect, the encapsulated (Mo)/Au(111) clusters exhibit higher selectivity for the formation of methane (reaction (2)) versus complete decomposition to surface carbon and sulfur (reaction (1)). A decrease in carbon deposition is usually considered a distinct advantage in most metal-catalyzed reactions as surface carbon often results in deactivation of the catalyst. For example, a Au/Ni surface alloy catalyst has been shown to have enhanced resistance to carbon poisoning in steam reforming reactions with hydrocarbons [47,51]. The modified behavior of the surface alloy is attributed to Au atoms blocking high reactivity sites on the supported Ni particles, thereby preventing the formation of carbon deposits [51]. Gold may play a similar role on (Mo)/Au(111) surfaces; however, the nearly inexhaustible supply of gold atoms from the Au(111) surface is likely to result in far greater coverages of Au atoms on the surface of annealed Mo nanoparticles. In this case, the Au capping atoms act intermediate between a physical barrier to adsorbed molecules and a chemical modifier of the (Mo)/Au(111) surfaces.

Another unusual property of the gold-encapsulated molybdenum nanoparticles is that they are virtually unreactive towards thiophene, while they are almost as reactive to methanethiol and hydrogen sulfide as bare molybdenum nanoparticles (see Fig. 8a–c). To better understand the chemical properties of the gold encapsulated (Mo)Au(111) surfaces, we first consider interactions of the molecules studied here with pure gold surfaces.

Thiophene, being a cyclic compound, does not chemically interact with the Au(111) surface [59]. At the same time, dehydrogenation of organothiols R-SH on the Au(111) and Au(100) surfaces is a well-known process responsible for the formation of self-assembled monolayers of thiolates R-S-Au [60]. In the case of alkanethiols $\text{CH}_3(\text{CH}_2)_n\text{SH}$, their sticking probability for dissociative chemisorption on both Au(111) and Au(100) surfaces decreases dramatically with decreasing chain length n [61]. In the case of CH_3SH ($n = 1$), only moderate dehydrogenation was detected on the Au(111) surface under UHV conditions and monolayer coverages [59] (similar to the conditions in our studies). The dissociation of H_2S ($n = 0$) has never been observed on gold surfaces [62,63], although theoretical calculations show that such dissociation is slightly more favorable energetically than that of methanethiol [64].

The gold atoms capping the Mo nanoparticles are likely to be coordinatively unsaturated and more reactive than atoms on close-packed Au(111) or Au(100) surfaces. We propose that hydrogen sulfide and methanethiol form thiolate intermediates (HS- and $\text{CH}_3\text{S-}$) on the gold covered (Mo)/Au(111) surface. The formation of R-S-Au thiolate intermediates [64] keeps the molecules tethered to the (Mo)/Au(111) surface during TPD experiments until the temperature is sufficiently high to promote mobility of the Au atoms and expose Mo sites. The latter react with the sulfur head group of the adsorbed thiolates to form a S-Mo bond and reaction products which desorb or deposit on the surface of the nanoparticles, e.g., $\text{H}_{(\text{a})}$, $\text{H}_{2(\text{g})}$, $\text{C}_{(\text{a})}$, and $\text{CH}_{4(\text{g})}$. As the surface of the Mo nanoparticle becomes sulfided, gold atoms are expelled back to the Au(111) surface (see Fig. 4). Thiophene, on the other hand, is only weakly physisorbed on the gold-encapsulated surface and most likely desorbs before it can react with molybdenum. The dissociation of thiophene would also require a larger active site (ensemble of Mo atoms), which may be sterically inaccessible in the presence of Au atoms on the Mo surface. [24,54]. These two factors make it highly improbable for thiophene to react with molybdenum on a gold-encapsulated surface except when the initial coverage of the Au atoms is low (Fig. 8c and d).

In a similar manner, the increase of the methane yield from methanethiol caused by the gold encapsulation can also be explained by limited access to active sites on the Mo surface. Even if the sulfur atom of a methanethiol molecule has reached Mo atoms through the gold film, further dehydrogenation of the CH₃ group may be hindered by the presence of Au atoms in neighboring sites. In this situation, the CH₃ group is more likely to react with surface hydrogen and desorb as CH₄. The surface hydrogen can originate from the S-H bond which is broken in forming the gold thiolate or the dehydrogenation of a fraction of the adsorbed methyl groups. Due to the limited sensitivity of the mass spectrometer, we were not able to distinguish between these two options.

4. Summary

Mo nanoparticles were formed on Au(111), and their reactivity towards H₂S, CH₃SH, and C₄H₄S was studied. STM images have shown that the nanoparticles formed by UV-CVD nucleate preferentially at the step edges. Gold migrates to the surfaces of the Mo nanoparticles when the sample is annealed above 300 K, which is a reflection of the surface free energy differences between Mo and Au. Gold atoms required for the encapsulation of the Mo particles are consumed from the step edges of the Au(111) surface. This leads to the formation of etching bays behind the lines of the Mo nanoparticles nucleated at the step edges. Upon exposure to H₂S, Mo reacts to form MoS_x and the gold atoms are expelled from the clusters back to the terraces. According to STM images, the nanoparticle morphology remains unchanged following this reaction.

Reactivity studies of bare Mo nanoparticles prepared by PVD on Au(111) have shown reactivity patterns similar to that of the Mo(110) surface. Each of the S-containing compounds dissociated completely on the Mo/Au(111) surface producing mainly hydrogen. Besides hydrogen, the only desorption product detected was methane evolving from CH₃SH with about 20% yield. The presence of gold atoms on the Mo nanoparticles significantly alters their reactivity. In the case of H₂S

and CH₃SH, the overall activity for desulfurization is unaffected by gold encapsulation, however, the relative yield of methane from CH₃SH increased to 60% on gold covered Mo particles. In contrast, gold-encapsulated Mo nanoparticles are relatively inert towards dissociation of thiophene. We propose that H₂S and CH₃SH form thiolate intermediates, HS⁻ and CH₃S⁻, that facilitate reaction on gold encapsulated Mo nanoparticles.

Acknowledgment

The authors would like to thank Dr. Tanhong Cai and Dr. Jan Hrbek for valuable discussions, and also for use of the STM and gold crystal. This research was carried out at Brookhaven National Laboratory under contract DE-AC02-98CH10086 with the US Department of Energy (Division of Chemical Sciences).

References

- [1] J.G. Speight, *The Chemistry and Technology of Petroleum*, second ed., New York, McGraw-Hill, 1991.
- [2] A.C. Stern, R.W. Boubel, D.B. Turner, D.L. Fox, *Fundamentals of Air Pollution*, second ed., FL Academic Press, Orlando, 1984.
- [3] K.G. Knudsen, B.H. Cooper, H. Topsøe, *Appl. Catal. A* 189 (1999) 205.
- [4] X. Lai, D.W. Goodman, *J. Mol. Catal. A* 162 (2000) 33, and references therein.
- [5] U. Heiz, W.-D. Schneider, in: K.-H. Meiwes-Broer (Ed.), *Metal Clusters at Surfaces: Structure, Quantum Properties, Physical Chemistry*, Springer, Berlin, 2000, pp. 237–274, and references therein.
- [6] V.I. Bukhtiyarov, M.G. Slin'ko, *Russian Chem. Rev.* 70 (2001) 147, and references therein.
- [7] H.J. Freund, M. Baumer, J. Libuda, T. Risse, G. Rupprechter, S. Shaikhutdinov, *J. Catal.* 216 (2003) 223.
- [8] R. Schlögl, S.B.A. Hamid, *Angew. Chem. Int. Ed.* 43 (2004) 1628, and references therein.
- [9] S. Helveg, J.V. Lauritsen, E. Laegsgaard, I. Stensgaard, J.K. Nørskov, B.S. Clausen, H. Topsøe, F. Besenbacher, *Phys. Rev. Lett.* 84 (2000) 951.
- [10] B. Hammer, Y. Morikawa, J.K. Nørskov, *Phys. Rev. Lett.* 76 (1996) 2141.
- [11] J.V. Barth, H. Brune, G. Ertl, R.J. Behm, *Phys. Rev. B* 42 (1990) 9307.
- [12] C.J. Baddeley, R.M. Ormerod, A.W. Stephenson, R.M. Lambert, *J. Phys. Chem.* 99 (1995) 5146.

- [13] B. Voigtlander, G. Meyer, N.M. Amer, Phys. Rev. B 44 (1991) 10354.
- [14] S. Padovani, F. Scheurer, J.P. Bucher, Europhys. Lett. 45 (1999) 327.
- [15] D.D. Chambliss, R.J. Wilson, S. Chiang, Phys. Rev. Lett. 66 (1991) 1721.
- [16] J.A. Rodriguez, J. Dvorak, T. Jirsak, J. Hrbek, Surf. Sci. 490 (2001) 315.
- [17] Z. Song, T. Cai, J.A. Rodriguez, J. Hrbek, A.S.Y. Chan, C.M. Friend, J. Phys. Chem. B 107 (2003) 1036.
- [18] J.A. Rodriguez, Surf. Sci. Rep. 24 (1996) 232.
- [19] I. Chado, F. Scheurer, J.P. Bucher, Phys. Rev. B 64 (2001) 094410.
- [20] T.B. Massalski, H. Okamoto, P.R. Subramanian, L. Kacprzak (Eds.), Binary Alloy Phase Diagrams, Materials Park, Ohio, ASM International, 1990.
- [21] M.V. Bollinger, J.V. Lauritsen, K.W. Jacobsen, J.K. Norskov, S. Helveg, F. Besenbacher, Phys. Rev. Lett. 87 (2001) 196803.
- [22] M.M. Biener, C.M. Friend, Surf. Sci. 559 (2004) L173.
- [23] J.A. Rodriguez, J. Dvorak, T. Jirsak, Surf. Sci. 457 (2000) L413.
- [24] J.T. Roberts, C.M. Friend, Surf. Sci. 186 (1987) 201.
- [25] H.H. Huang, C.S. Sreekanth, C.S. Seet, X. Jiang, G.Q. Xu, Surf. Sci. 365 (1996) 769.
- [26] Z.C. Ying, W. Ho, J. Chem. Phys. 94 (1991) 5701.
- [27] S.K. So, W. Ho, J. Chem. Phys. 95 (1991) 656.
- [28] T.A. Germer, W. Ho, J. Chem. Phys. 89 (1988) 562.
- [29] N.A. Beach, H.B. Gray, J. Am. Chem. Soc. 90 (1968) 5713.
- [30] A. Zangwill, Physics at Surfaces, Cambridge University Press, Cambridge, 1988.
- [31] D.V. Potapenko, J.M. Horn, M.G. White, in preparation.
- [32] P. Liu, J.A. Rodriguez, J.T. Muckerman, J. Hrbek, Surf. Sci. 530 (2003) L313.
- [33] L.Z. Mezey, J. Gibei, Jpn. J. Appl. Phys. 21 (1982) 1569.
- [34] P. Liu, J.A. Rodriguez, J.T. Muckerman, J. Hrbek, Phys. Rev. B 67 (2003) 155416.
- [35] A.V. Ruban, H.L. Skriver, J.K. Norskov, Phys. Rev. B 59 (1999) 15990.
- [36] R.Q. Hwang, M.C. Bartelt, Chem. Rev. 97 (1997) 1063.
- [37] A.K. Schmid, D. Altan, H. Itoh, B. Heinrich, T. Ichinokawa, J. Kirschner, Phys. Rev. B 48 (1993) 2855.
- [38] J.d.l. Figueroa, J.E. Prieto, G. Kostka, S. Muller, C. Ocal, R. Miranda, K. Heinz, Surf. Sci. 349 (1996) L139.
- [39] C.G. Zimmermann, M. Yeadon, K. Nordlund, J.M. Gibson, R.S. Averback, Phys. Rev. Lett. 83 (1999) 1163.
- [40] C. Nagl, E. Platzgummer, M. Schmid, P. Varga, S. Speller, W. Heiland, Phys. Rev. Lett. 75 (1995) 2976.
- [41] E.I. Altman, R.J. Colton, Surf. Sci. Lett. 304 (1994) L400.
- [42] S.-L. Chang, J.-M. Wen, P.A. Thiel, S. Gunther, J.A. Meyer, R.J. Behm, Phys. Rev. B 53 (1996) 13747.
- [43] G.A. Attard, D.A. King, Surf. Sci. 188 (1987) 589.
- [44] J. Takahashi, M. Sasaki, S. Suzuki, S. Sato, T. Abukawa, S. Kono, J. Osterwalder, Surf. Sci. 304 (1994) 65.
- [45] X.K. Shu, P. Jiang, J.G. Che, Surf. Sci. 545 (2003) 199, and references therein.
- [46] D. Singh, H. Krakauer, Surf. Sci. 216 (1989) 303.
- [47] F. Besenbacher, I. Choredorff, B.S. Clausen, B. Hammer, A.M. Molenbroek, I. Stensgaard, Science 279 (1998) 1913.
- [48] C.T. Campbell, Annu. Rev. Phys. Chem. 41 (1990) 775, and references therein.
- [49] J.R. Cerda, F. Soria, F.J. Palomares, P.L.d. Andres, Surf. Sci. 269/270 (1992) 713.
- [50] D. Wu, W.K. Lau, Z.Q. He, Y.J. Feng, M.S. Altman, C.T. Chan, Phys. Rev. B 62 (2000) 8366.
- [51] A.M. Molenbroek, J.K. Norskov, B.S. Clausen, J. Phys. Chem. B 105 (2001) 5450.
- [52] W.S.M. Werner, Surf. Interface Anal. 31 (2001) 141.
- [53] E. Stenhagen, S. Abrahamsson, F.W. McLafferty (Eds.), Atlas of Mass Spectral Data, John Wiley, New York, 1969.
- [54] F. Zaera, E.B. Kollin, J.L. Gland, Surf. Sci. 184 (1987) 75.
- [55] D.G. Kelly, M. Salmeron, G.A. Somorjai, Surf. Sci. 175 (1986) 465.
- [56] A.C. Liu, C.M. Friend, J. Am. Chem. Soc. 113 (1991) 820.
- [57] J.T. Roberts, C.M. Friend, J. Am. Chem. Soc. 108 (1986) 7204.
- [58] B.C. Wiegand, P. Uvdal, C.M. Friend, Surf. Sci. 279 (1992) 105.
- [59] G. Liu, J.A. Rodriguez, J. Dvorak, J. Hrbek, T. Jirsak, Surf. Sci. 505 (2002) 295.
- [60] A. Ulman, Self-Assembled Monolayer of Thiols, Academic Press, New York, 1998.
- [61] L.H. Dubois, B.R. Zegarski, R.G. Nuzzo, J. Chem. Phys. 98 (1993) 678.
- [62] V. Bondzie, S. Dixon-Warren, Y. Yu, J. Chem. Phys. 111 (1999) 10670.
- [63] A.J. Leavitt, T.B. Beebe Jr., Surf. Sci. 314 (1994) 23.
- [64] J. Gottschalck, B. Hammer, J. Chem. Phys. 116 (2002) 784.